Heidbach, O., Ben-Avraham, Z. (2007): Stress evolution and seismic hazard of the Dead Sea Fault System. - Earth and Planetary Science Letters, 257, 1-2, 299-312

DOI: 10.1016/j.epsl.2007.02.042

Earth and Planetary Science Letters 257 (2007) 299-312

Stress evolution and seismic hazard of the Dead Sea Fault System

Oliver Heidbach[a,*], Zvi Ben-Avraham[b]

[a] *Geophysical Institute, Karlsruhe University, Hertzstr.16, 76187 Karlsruhe Germany*
[b] *Department of Geophysics and Planetary Science, Tel Aviv University, P.O.B. 39040, Ramat Aviv, Tel Aviv, 69978, Israel*

Received 5 January 2006; received in revised form 26 February 2007; accepted 26 February 2007
Available online 6 March 2007
Editor: R.D. van der Hilst

Abstract

We calculated the stress evolution for the central part of the Dead Sea Fault System (30.5°N–34.5°N) from 551 to 2005 through modelling the static stress changes due to 14 historical earthquakes with $M_S \geq 6.0$ superimposed by tectonic loading from relative plate motion. From the results of our numerical models, we identified two segments with high positive changes in Coulomb failure stress (ΔCFS) exceeding 4 MPa, a ~90-km-long segment of the Jordan Fault south of the Sea of Galilee and a ~30-km-long segment east of the Dead Sea. These segments could result in $M_S = 7.4$ and $M_S = 6.8$ earthquakes, respectively. In contrast to similar stress evolution models of other continental transform faults, our results support only partly the hypothesis that coseismically induced static stress changes control the spatial succession of earthquakes. We calculated on each rupture plane the mean of ΔCFS and the maximum ΔCFS due to the stress changes of all preceding earthquakes. The results of the calculated mean ΔCFS values reveal that only 6 out of 13 earthquakes could have been triggered the subsequent earthquake. From the analysis of the maximum ΔCFS values, we find that 8 out of 13 earthquakes could have triggered the subsequent earthquake. Since our model results are sensitive to location and magnitude of historical earthquakes and the tectonic loading rates of the fault segments, we emphasize the need for further paleoseismological studies and current slip rate estimation from continuously observing GPS arrays and geological investigations. Taking into account that six large cities (Beirut, Damascus, Haifa, Tel Aviv, Amman, and Jerusalem) are in close proximity with distances between 30 and 150 km to the Jordan segment, the seismic risk is probably higher than accounted before.

Keywords: earthquake triggering; Dead Sea Fault; seismotectonics; Coulomb failure stress

1. Introduction

Seismic hazard and its variation in time is linked to the contemporary state of stress of seismically active fault systems. The stress evolution of a fault is mainly controlled by the tectonic loading rate due to plate motion and stress perturbations induced by co- and post-seismic stress transfer [1, 2]. Models incorporating coseismically induced static stress changes and tectonic loading have been successfully applied to explain earthquake sequences, e.g. along the East Anatolian Fault system [3], in western Turkey [4], along the North Anatolian Fault system [5–7] and in Southern California [8–10]. These findings contributed fundamental information for the estimation of earthquake probabilities and seismic hazard assessment, e.g. for the Marmara region south of Istanbul, where a strong earthquake is expected [5, 11, 12], and for Southern California [13]. In contrast to these regions, where sequences of strong earthquakes have been observed in the last century, seismic records of the same period from the central part of the Dead Sea Fault System (DSFS) between 30.5°N and 34.5°N exhibit only two earthquakes with $M_S \geq 6.0$: The 1927 earthquake ($M_S = 6.2$) at the north-western rim of the Dead Sea and the 1956 earthquake ($M_S = 6.0$) southwest of Beirut (Fig. 1). The last strong earthquake took place in 1837 ($M_S = 7.4$) in the Hula basin north of the Sea of Galilee. The long recurrence intervals for strong earthquakes in the order of 10^3–10^4 years [14–

* Corresponding author. Tel.: +49 721 6084609; fax: +49 721 71173.
E-mail address: oliver.heidbach@gpi.uni-karlsruhe.de (O. Heidbach)

18] are due to low slip rates along the various DSFS segments between 1 and 7 mm/yr [19–23]. However, the dense population since historical times as well as several paleoseismological and archaeological investigations provide comprehensive catalogues of large historical earthquakes for the last 2000 years [14, 15, 18, 19, 24–32]. Taking into account that six major cities (Beirut, Damascus, Haifa, Tel Aviv, Amman, and Jerusalem) are located close to the DSFS (<50 km), the analysis of its stress evolution provides fundamental information for the evaluation of seismic hazard and seismic risk.

Here we present a numerical model for the evolution of stress along the central DSFS (30.5°N–34.5°N) for the last 1450 years including coseismic stress changes due to a sequence of 14 $M_S \geq 6.0$ earthquakes and tectonic loading due to plate motion. We test the hypothesis whether the earthquake sequence could have been triggered by the coseismically induced static stress changes. We also calculate the evolution of stress in terms of changes of Coulomb failure stress (ΔCFS) for different time steps taking into account the varying strike of the fault segments. The final time step in the year 2005 (of the numerical stress evolution calculations) reveals the current state of stress and enables us to assess the seismic hazard for individual fault segments.

2. Neotectonics and historical seismicity

The DSFS represents a continental left-lateral strike–slip fault system which separates the Arabia plate from the Africa plate (Fig. 1). A displacement of 105 km

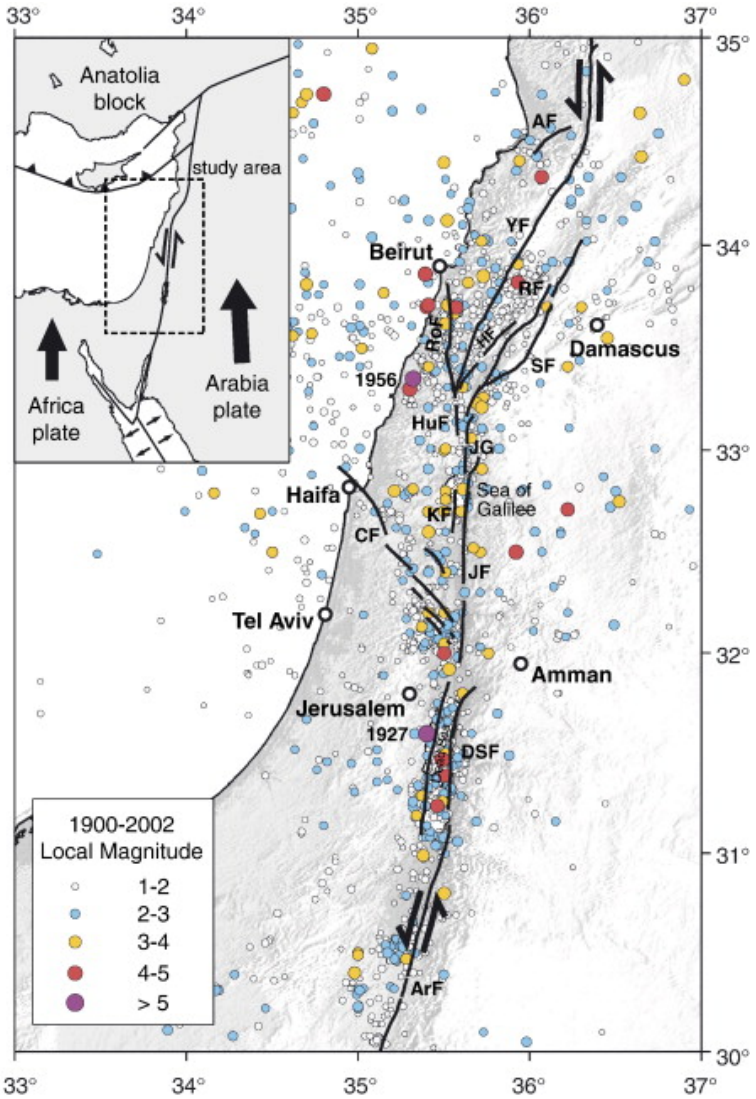

Figure 1. Recorded seismicity of the study area from 1900 to 2002 (Geophysical Institute of Israel, available online at http://www.gii.co.il). Black lines are the active faults. Abbreviations are: AF = Akar Fault, ArF = Arava Fault, CF = Carmel Fault, DSF = Dead Sea Fault, HF = Hasbaya Fault, HuF = Hula Fault, JF = Jordan Fault, JG = Jordan Gorge, KF = Kinnereth Fault, RoF = Roum Fault, RF = Rachaiya Fault, SF = Serghaya Fault, YF = Yammouneh Fault. The locations of the two $M_L \geq 6.0$ earthquakes from the 20th century are indicated by the year numbers.

occurred along this 1000-km-long boundary since the late Miocene [33]. Our study area is the central part, from 30.5°N to 34.5°N, including the Dead Sea and the Sea of Galilee connected by the Jordan Fault. At the Dead Sea, the Jordan fault splits into a western and a eastern segment separated by the Dead Sea pull-apart basin. Further south, the Arava Fault connects the DSFS to the Gulf of Aqaba [34]. North of the Sea of Galilee, the DSFS splits into several branches. From west to east these branches are: the Roum Fault, the Yammouneh Fault, the Hasbaya Fault, the Rachaiya Fault, and the Serghaya Fault (Fig. 1).

2.1. Fault kinematics

It has been recognized that the total left-lateral slip of ~105 km south of the Sea of Galilee is not older than 18 Ma [33, 35, 36]. This gives a minimum slip rate of 5.8 mm/yr. A review of the overall DSFS kinematics for the last ~5 Ma from Westaway [37] states that the system had an average slip rate of ~7 mm/yr. For the Late Pleistocene and Holocene Klinger et al. [23] estimated a slip rate of 4.0±2 mm/yr for the Arava Fault between the Gulf of Aqaba and the Dead Sea. From continuous GPS observations in Israel and Jordan, Wdowinski et al. [20] observed a contemporary slip rate of 3.3±4 mm/yr for the Jordan Fault.

Further north Meghraoui et al. [32] found a slip rate of 6.9±0.1 mm/yr for the Missyaf segment in Syria north of the Yammouneh Fault from paleoseismologic and archaeological evidence. This is slightly higher than the Late Pleistocene–Holocene slip rate of 3.8–6.4 mm/yr for the Yammouneh Fault from Daëron et al. [38]. However, the findings of Meghraoui et al. [32] represent an average slip rate from ~2000 years including a succession of four strong earthquakes, and thus probably rep-

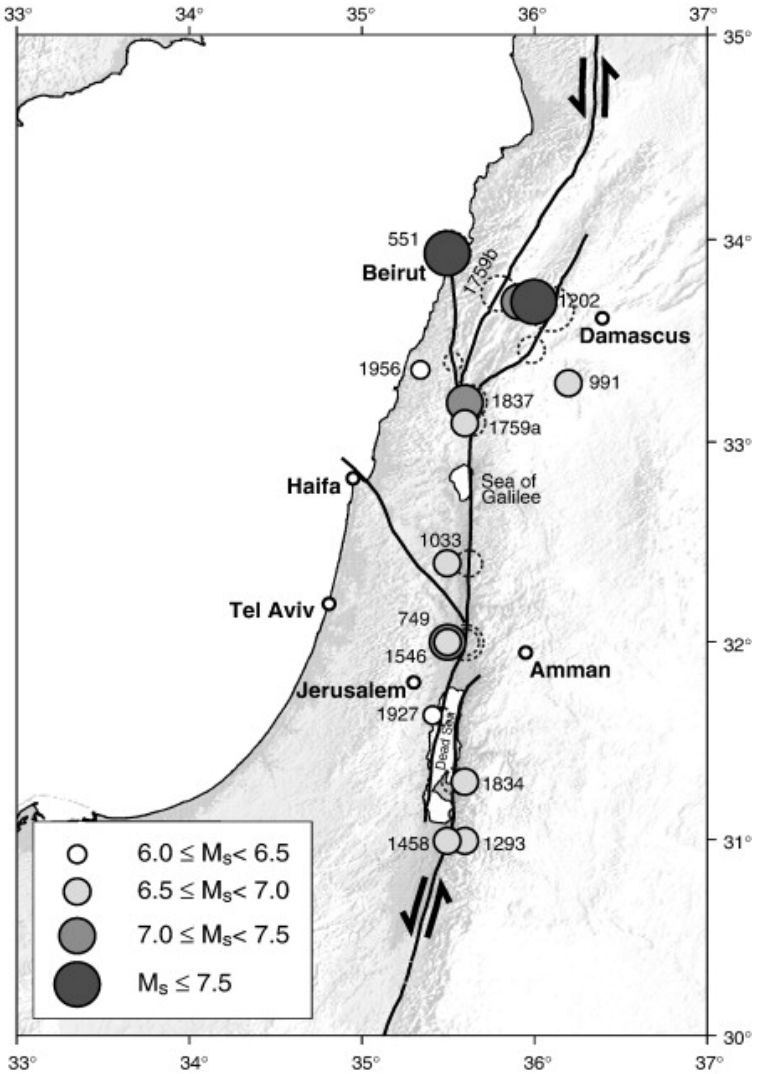

Figure 2. Location and year date of the 14 historical earthquakes ($M_S \geq 6.0$) along the Dead Sea Fault System (DSFS) of the last 1500 years (for details see Table 1). Dashed circles indicate the locations after shifting the epicentres onto the nearest major active fault.

resents an upper bound.

These findings contradict the older results which assume that the Yammouneh Fault as well as the faults further east (Hasbaya Fault, Rachaiya Fault, and Serghaya Fault) are inactive [22, 39]. This is also in contrast to the findings of Gomez et al. [40]. They find from the analysis of Late Pleistocene and Holocene lake deposits slip rates between 1 and 2 mm/yr on the Serghaya Fault including large offsets from historical earthquakes.

Walley [41] states that the Yammouneh Fault shows, in recent geological times, small slip rates between 0.8 and 1.6 mm/yr. He proposes that the faults further east have been active in Pre-Pliocene, but that the activity shifted to the Roum Fault. The Roum Fault is the northern prolongation of the DSFS and strikes N10°W (Fig. 1). Even though its surface trace disappears south of Beirut it shows recent tectonic activity [42]. River channel displacements for the last 5 Ma reveal offsets of ~8 km in the south and smaller ones in the order of a few kilometres in the north [42, 43]. This would give a maximum slip rate of 1.6 mm/yr for the Roum Fault. Thus, the Roum Fault can take up only a minor portion of the total relative plate motion of ~5 mm/yr between the Arabia plate and the Africa plate.

We assume for our model that the Yammouneh Fault is the most active fault with slip rates of 3–4 mm/yr. The Roum Fault and the Serghaya Fault are less active and have slip rates of ~1 mm/yr, whereas the Hasbaya Fault and the Rachaiya Fault are assumed to be inactive.

South of this complex system the Jordan Gauge, the small fault segment just north of the Sea of Galilee, shows a minimum slip rates for the Holocene of 3 mm/yr [19] which fits to the geodetically observed slip rate of 3.3±0.4 mm/yr [20]. Another seismically active fault is the Carmel Fault. It strikes N40°W, starts north of the Dead Sea, and continues offshore crossing Haifa Bay [44, 45] (Fig. 1). Here we assume a slip rate of 1 mm/yr for our model.

2.2. Historical earthquakes

Besides the instrumentally recorded earthquakes of the years 1927 and 1956 we compiled historical earthquakes using various catalogues from year 551 onwards [14, 15, 18, 24–27, 29]. In total we identified 14 historical earthquakes with $M_S \geq 6.0$ (Fig. 2 and Table 1). We are aware that these compilations have limited accuracy with respect to the given epicentre location and the estimated magnitude from the observed intensities. Furthermore, the publications on historical earthquakes are not consistent since they account for different historical documents and their interpretations. Our selection of earthquake location and magnitude is not an attempt to compile a new catalogue, but a selection of historical earthquake data where the majority of publications are in agreement. The data for the historical earthquakes used for the modelling are summarized in Table 1.

Since no detailed source mechanisms are known for historical earthquakes, we made the following assumptions: (1) They occurred along the known major active faults. We projected the epicentres onto the nearest major active fault following the findings of Garfunkel [21] and Ambraseys and Jackson [46] who found a good correlation of large earthquakes with major active faults in the region (Fig. 2). The mean relocation distance of ~10 km indicates that this is a reasonable assumption. (2) The slip directions of the earthquakes follow the strike of the associated faults and are horizontal. (3) The dip of the faults is vertical which is in agreement with the available focal mechanisms solutions of recorded smaller earthquakes [47,48]. (4) The locking depth is $w = 12.5$ km and defines the vertical extension of the rupture plane for all earthquakes. This is in agreement with average focal depths of 8.7 km for earthquakes in the study area with $M_L \geq 3.0$ recorded in the period from 1982 to 2002 (Israel seismological network of the Geophysical Institute of Israel, available online at http://www.gii.co.il). (5) The slip distribution along the rupture plane is uniform and bi-directional from the epicentre for all earthquakes, except the 551 and the 1837 earthquake.

For the 551 earthquake we extend the rupture plane only in southern direction from the reported epicentre since no fault trace has been detected offshore [42, 43].

Table 1
Model parameters for the historical earthquakes

Year (AD)	Lat. (deg N)	Lon. (deg E)	M_S	l[a] (km)	u[b] (m)
551	33.9	35.5	7.5	115	3.8
749	32.0	35.5	7.3	79	2.8
991	33.3	36.2	6.7	25	1.1
1033	32.4	35.5	6.7	25	1.1
1202	33.7	36.0	7.5	115	3.8
1293	31.0	35.6	6.8	31	1.3
1458	31.0	35.5	6.8	31	1.3
1546	32.0	35.5	7.0	45	1.7
1759a	33.1	35.6	6.8	31	1.3
1759b	33.7	35.9	7.4	95	3.2
1834	31.3	35.6	6.3	12	0.6
1837	33.2	35.6	7.1	54	2.0
1927	31.6	35.4	6.2	11	0.5
1956	33.35	35.32	6.0	7	0.4

[a] Length of the ruptured fault segment assuming that $M_L \approx M_S$ in case only M_L was given in the sources.

[b] Displacement along the fault segment assuming a locking depth w of 12.5 km.

For the 1837 earthquake, we extend the rupture plane only in northern direction along the Yammouneh Fault from the reported epicentre. Assuming that the Roum Fault and the Serghaya Fault are less active it is more likely that the 1837 earthquake occurred on the Yammouneh Fault. An alternative fault could have been the Jordan Gauge, but this is less likely since this is not a through-going structure and does not provide the needed rupture plane length of 54 km for the $M_S \geq 7.1$ earthquake. This assumption is in agreement with Marco et al. [19]. They assume that the two historical earthquakes which are seen in their paleoseismological trenches crossing the Jordan Gorge are the 1202 earthquake and the 1759a earthquake. Even though Ambraseys [24] states that there is no clear evidence whether the 1837 earthquake occurred on the Roum Fault or the Yammouneh Fault we decided to place it on the latter since (a) the slip rates on the Roum Fault are too small to accumulate enough strain after the 551 earthquake and (b) a major aftershocks of the 1837 occurred slightly east of the Yammouneh Fault [24].

3. Stress evolution model

To model the static stress field changes due to the sequence of the 14 historical earthquakes and the tectonic loading we applied the boundary element method for a 3D elastic half space using the software Poly3D of Thomas [49]. For the DSFS model geometry we implemented the major active segments and neglected smaller, presumably inactive fault branches such as the Hasbaya, Kinnereth [50], and Rachaiya Fault (Figs. 1 and 2). For the tectonic loading we assume a slip rate of 5 mm/yr between the Africa plate and the Arabia plate. Given the discussion in the previously presented fault kinematics section we assign to the Carmel Fault, the Roum Fault, and the Serghaya Fault a slip rate of 1 mm/yr. The Yammouneh Fault is given slip rates between 3 and 5 mm/yr. The Arava Fault and the Jordan Fault is given a slip rate of 5 mm/yr and, for the western and eastern fault segments along the Dead Sea, the slip rates decrease from 4 mm/yr to 0 at the ends of the faults (Fig. 4).

The second boundary condition comes from the coseismic slip on the rupture plane. The rupture plane length l is calculated with the empirical formula of Ambraseys and Jackson [46]

$$\log l[\mathrm{km}] = 0.82 M_S - 4.09 \,. \quad (1)$$

The coseismic displacement u along the rupture plane is given with the formula

$$u = M_0/(G \cdot A) \quad (2)$$

where A is the area of the rupture plane ($A = lw$), G the shear modulus and M_0 the seismic moment. According to Ambraseys and Jackson [46], M_0 is given with the empirical formula

$$\log M_0 = 1.5 M_S + 9.0 \,. \quad (3)$$

The results of the calculations for the rupture plane lengths l and the coseismic displacements u for each earthquake are summarized in Table 1 and represented in Fig. 3.

In addition to the coseismic slip of the earthquakes,

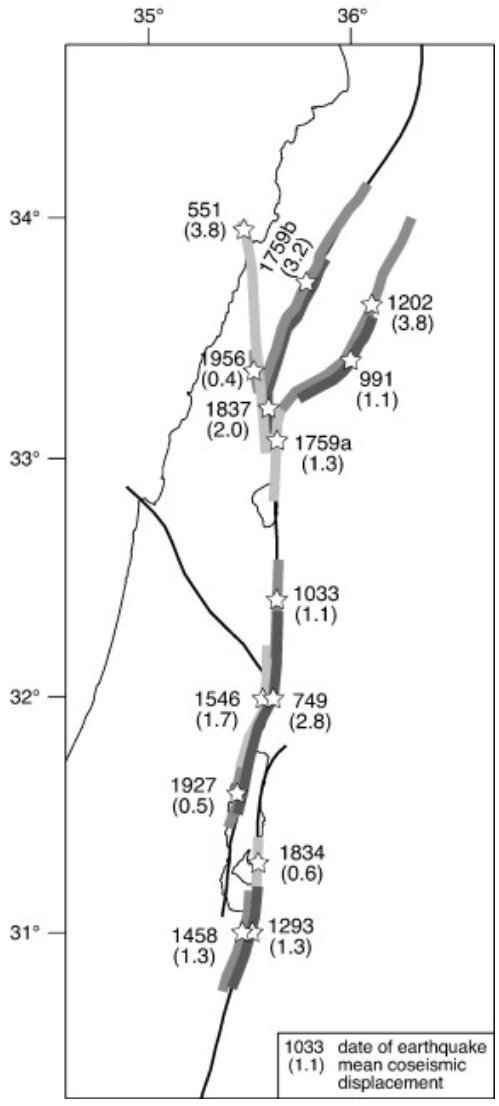

Figure 3. Epicentres (stars) and rupture lengths (grey thick lines) of the 14 historical earthquakes along the Dead Sea Fault System (thin black line). The average coseismic displacement on the rupture planes is calculated from Eqs. (1) and (2) in the text.

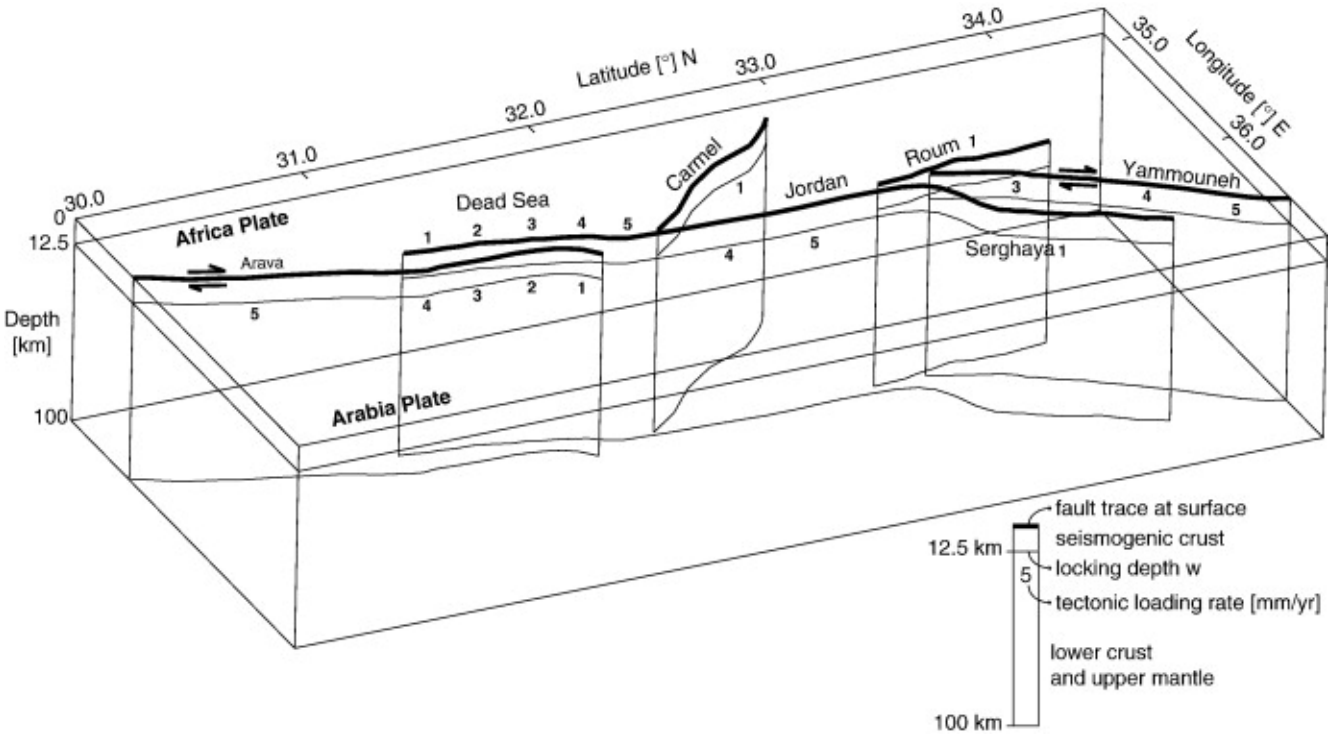

Figure 4. 3D model sketch of the study area. The numbers at the various fault segments give the applied tectonic loading rate (slip rate) in mm/yr below the locking depth *w* at 12.5 km.

the ongoing relative movement between the Arabia plate and the Africa plate produces stress loading along the seismogenic part of the fault, i.e. the upper 12.5 km. We model this tectonic loading by increasing the fault slip rates in steps of 1 mm/yr from zero at 12.5 km depth (locking depth w) to the full relative displacement rate for each segment of the DSFS at 17.5 km depth. From 17.5 to 100 km depth the full slip rates are applied (Fig. 4).

From the resulting stress field of the boundary element model we calculated the change of Coulomb failure stress (ΔCFS) on the rupture plane of the subsequent earthquake (Table 1). Reasenberg and Simpson [51] define ΔCFS as

$$\Delta\mathrm{CFS} = \Delta\tau + \mu'\Delta\sigma_n \quad (4)$$

where $\Delta\tau$ is the change in shear stress (positive in slip direction of the subsequent earthquake), $\Delta\sigma_n$ the change of normal stress perpendicular to the rupture plane of the subsequent earthquake (negative for compression), and μ' the apparent coefficient of friction. We performed all calculations with a shear modulus of $G = 33$ GPa, a Poisson ratio of 0.25 for the 3D elastic half space, and an apparent friction coefficient of $\mu' = 0.4$.

In contrast to the commonly used ΔCFS representations in map view (e.g., [5, 7, 8]), we follow the concept of Nalbant et al. [3] displaying ΔCFS only at the faults. These ΔCFS values are calculated at a depth of 6.25 km in 1-km spacing, taking into account the varying orientation of the rupture plane. From these calculations, the stress evolution in terms of ΔCFS values at different stages of the historical earthquake sequence is displayed in profiles along the fault strike of the various DSFS segments (Fig. 5).

4. Results

We analysed the numerical model results for the evolution of stress from two different perspectives: (1) *Stress triggering:* Could the sum of the coseismically induced stress changes from the preceding earthquakes have triggered the subsequent earthquake? (2) *Present-day stress state:* We calculated for each fault segment the present-day stress state considering the stress evolution for the years 551–2005 including the tectonic loading and the coseismically induced static stress changes.

4.1. Static stress triggering

From the coseismically induced stress changes of the preceding earthquakes we calculated along the rupture plane of the succeeding earthquake the mean ΔCFS and

the maximum ΔCFS value (Table 2). The results are classified according to the following scheme: If the rupture plane of the succeeding earthquake experienced a mean/maximum ΔCFS > 0.1 MPa the earthquake was classified as probably triggered by the static stress changes of the preceding earthquakes, while for a mean/max ΔCFS < 0.01 MPa triggering is unlikely. Given this classification, 8 out of 13 earthquakes show potential triggering due to the maximum ΔCFS values, and 6 out of 13 earthquakes due to mean ΔCFS values. The other earthquakes occur in regions with negative ΔCFS values between −0.03 and −10.51 MPa (Table 2).

4.2. Stress evolution

Evolution of stress along the DSFS is calculated for

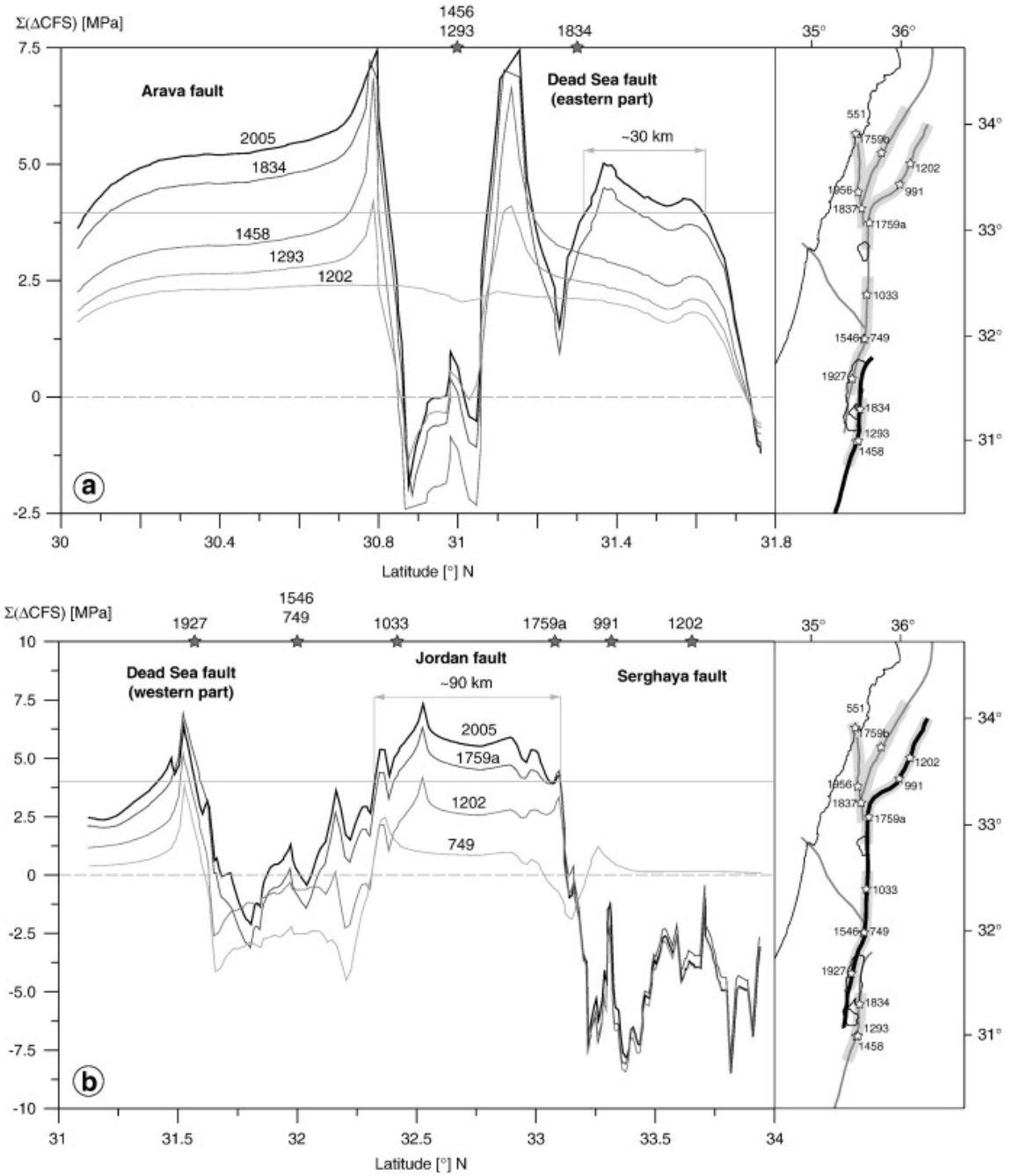

Figure 5. Evolution of ΔCFS for five fault zones along the Dead Sea Fault System (DSFS) from 551 (ΔCFS=0) to 2005. In order to suppress unrealistic edge effects at the endings of each rupture plane, the five last points are smoothed. Plotted segments are shown on the overview maps as thick black lines. Lines with increasing grey scale represent the stress state of the given year. Stars indicate the position of the earthquake. Dashed lines are the 0 ΔCFS level and the thin grey lines in panels a and b are the 4 MPa ΔCFS level. Note the increased ΔCFS values in year 2005 for a 30-km-long section of the eastern Dead Sea Fault (a) and a 90-km-long section for the Jordan Fault (b) which could according to Eq. (1) produce M_S =6.8 and M_S =7.4 earthquake, respectively.

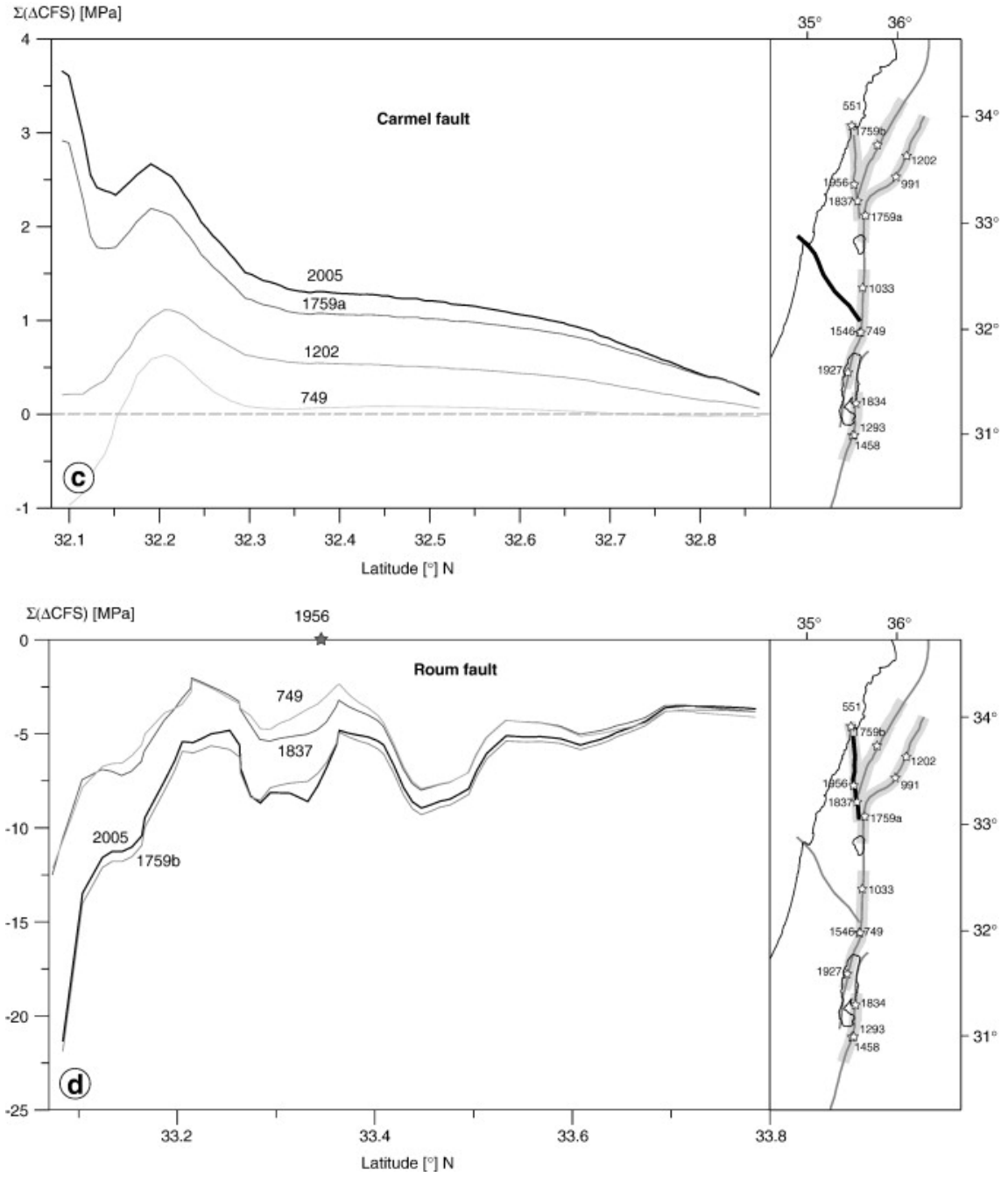

Figure 5. *(continued).*

various times including the effect of tectonic loading and coseismically induced stress changes. Fig. 5a–e display the results for the DSFS. The ΔCFS values for the stress evolution are also calculated in steps of 1 km, taking into account the varying orientations of the fault segments.

Fig. 5a shows the results for the Arava Fault and the eastern part of the Dead Sea Fault. The curves display the unloading effect caused by the 1293, 1458 and 1837 earthquake. For the last time step in 2005 the northern part of this segment along the eastern side of the Dead Sea has been loaded with ΔCFS > 4 MPa over a length of ~30 km. According to Eq. (1) this loading could result in a $M_S = 6.8$ earthquake. The high stress level of the Arava Fault south of 30.9°N is probably artificial. Historical earthquakes such as the 1068 earthquake with $M > 6.6$ [52, 53], which occurred outside the model boundary, probably unloaded this Arava Fault segment.

Fig. 5b displays the stress evolution for the western part of the Dead Sea Fault, the Jordan Fault and the Serghaya Fault. The curves show the unloading effect of the 749 earthquake on the western part of the Dead Sea

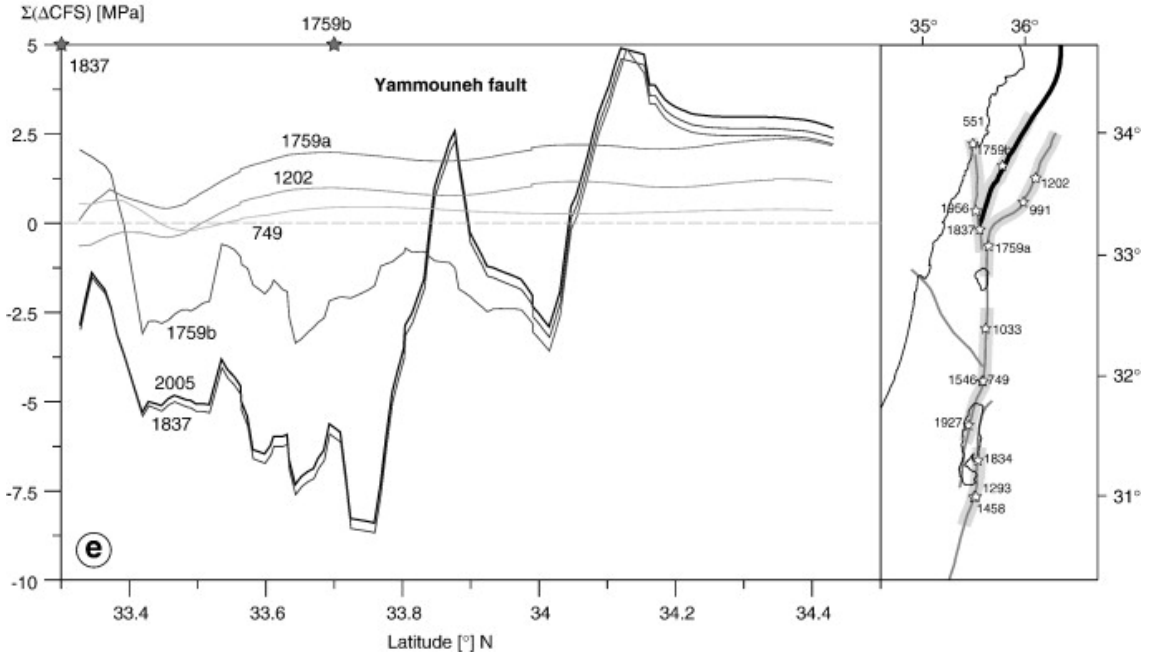

Figure 5. *(continued).*

Fault and the unloading of the Serghaya Fault due to the 1202 earthquake. The final time step of the stress evolution in 2005 indicates that the central segment of the Jordan Fault has accumulated ΔCFS > 4 MPa over a length of ~90 km. Following Eq. (1) this segment might generate a $M_S = 7.4$ earthquake.

Fig. 5c and d give the stress evolution for the Carmel Fault and the Roum Fault, respectively. The Carmel Fault shows small increases in positive ΔCFS values over time with the largest increase near the junction with the Jordan Fault. In contrast to that, the Roum Fault is fully unloaded. Due to the large 551 earthquake and the smaller one in 1956, the ΔCFS < −5 MPa (Fig. 5d).

Fig. 5e represents the stress evolution for the Yammouneh Fault. Here the major unloading effects result from the earthquakes of 1759b and 1837. Thus, the final stage of stress evolution in 2005 reveals an unloaded southern part of the Yammouneh Fault with negative ΔCFS values of ~−2.5 MPa or smaller. North of 34° the ΔCFS values increase to high positive values. However, this is probably an artificial result due to the proximity of the model boundary. The well-documented large historical earthquakes in the 12th century on the Gharb Fault [32,54] are located just north of our study area and probably unloaded the northern segment of the Yammouneh Fault.

The contemporary stress state in 2005 for all segments is summarized in Fig. 6. The areas, which are probably affected by large earthquakes outside our model boundary, were removed from this figure. The map shows that a ~90-km-long segment of the Jordan Fault and a ~30-km-long section of the eastern segment of the Dead Sea Fault have high potential for a future strong earthquake. Fig. 6 emphasizes the close proximity of several large cities to the segments with high ΔCFS values.

Table 2
Results of ΔCFS analysis

Year	Triggered[a]	Maximum ΔCFS[b] (MPa)	Triggered[a]	Mean ΔCFS[c] (MPa)
551				
749	+	0.02	+	0.01
991	+	0.35	+	0.09
1033	+	2.72	−	−0.72
1202	+	3.12	+	0.01
1293	+	0.03	+	0.01
1458	−	−0.03	−	−3.14
1546	−	−2.54	−	−3.46
1759a	−	−0.93	−	−4.92
1759b	+	0.36	−	−0.33
1834	+	0.49	+	0.32
1837	−	−1.52	−	−3.59
1927	+	4.75	+	0.06
1956	−	−7.58	−	−10.51

[a] '+': probable triggering due to the preceding earthquakes assuming a threshold value of ΔCFS > 0.01 MPa; '−': ΔCFS < −0.01 MPa.
[b] Maximum ΔCFS value along the rupture plane due to all preceding earthquakes.
[c] Mean ΔCFS value along the rupture plane due to all preceding earthquakes.

5. Discussion

The static stress-triggering hypothesis refers to the causal relationship between two subsequent earthquakes. This hypothesis has been successfully tested for

a succession of earthquakes in several continental strike–slip systems such as the North Anatolian Fault, East Anatolian Fault and parts of the San Andreas Fault [3–5, 9, 13]. Stein et al. [5] showed that 9 out of 10 earthquakes from a 20th century sequence of major earthquakes along the North Anatolian Fault are probably triggered by their precursors. In their study, the positive ΔCFS values at the epicentre of the following earthquake were, on average, 0.31 MPa. Furthermore, none of the epicentres showed negative ΔCFS values. In contrast to these findings, our ΔCFS results indicate only limited interaction between the earthquakes due to static stress change. Only 6 (mean ΔCFS values along the rupture plane), or 8 (maximum ΔCFS values on the rupture plane), of the 13 historical earthquakes can be addressed to static stress triggering assuming a threshold value of 0.01 MPa (Table 2). In our model the remaining 7 (mean ΔCFS), respectively 5 (maximum ΔCFS) earthquakes, are located in stress shadows, i.e., in areas where the sum of the coseismic stress changes from the preceding earthquakes is negative. The location of a large earthquake in the stress shadow of the preceding earthquakes has also been detected for the 1911 Morgan Hill earthquake in the San Francisco Bay area [55] and an earthquake doublet from 1997 in Kagoshima, Japan [56]. Furthermore, a recent global analysis of static stress triggering using shallow earthquakes (<50 km) of the CMT Harvard catalogue from 1976–2001 revealed that strike–slip earthquakes seem less in support of the triggering hypothesis [57]. We are aware that our research is only one possible scenario of stress evolution due to the high uncertainties in location and magnitude of the historical earthquakes, local effects caused by the probably oversimplified fault geometry of the model, and the assumed slip distribution and sense of slip. Thus, in the following we discuss a number of possible ways to explain the deviation from the static stress-triggering hypothesis.

(1) *Large uncertainties in location and magnitude of the historical earthquakes:* This is a severe problem which cannot be addressed until more paleoseismo-

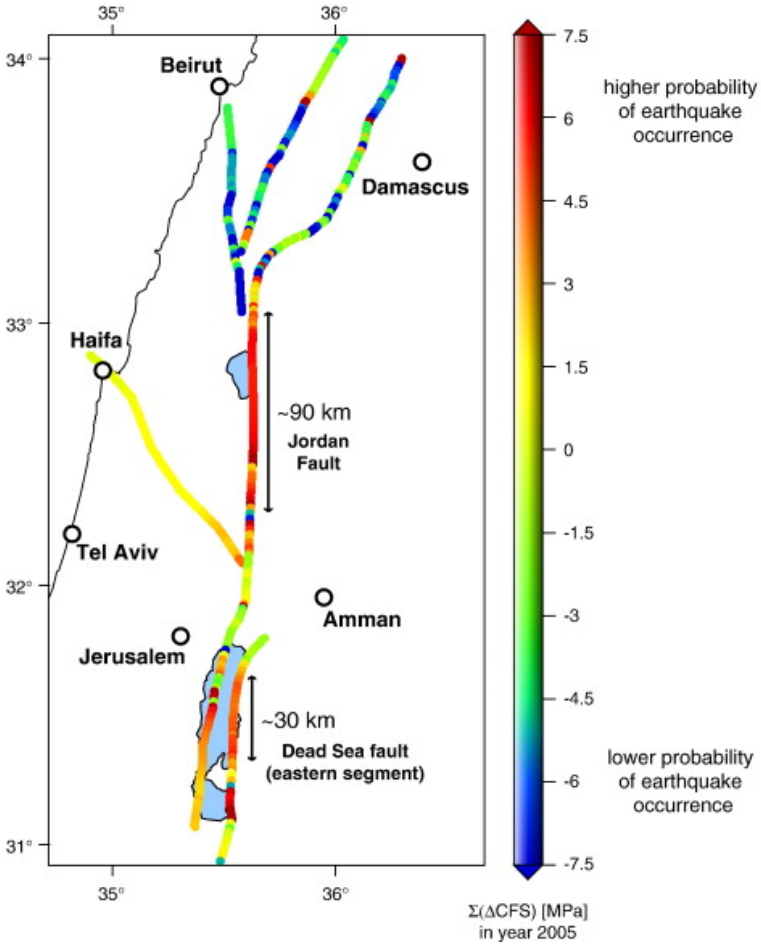

Figure 6. Present-day stress state of the Dead Sea Fault System. Displayed are the cumulative ΔCFS values calculated for the varying orientation of each fault in 1-km steps. The ΔCFS values include the coseismically induced stress changes superimposed by the stress effect from tectonic loading for the period from 551 to 2005. Note the large positive values along the Jordan Fault and the eastern segment of the Dead Sea Fault.

logical and archaeological data are available. For instance, very recent findings from paleoseismological investigations along the Serghaya and Yammouneh Fault indicate that the 1202 earthquake probably occurred on the Yammouneh Fault and the 1759b earthquake on the Serghaya Fault [58]. We implemented these two earthquakes the other way around in our model following our model assumption to relocate each earthquake to the nearest active fault segment. However, this does not influence the final present stress state since both earthquakes differ only by 0.1 in magnitude and have the same latitude location. Thus, the stress evolution of the Yammouneh Fault and the Serghaya Fault would take a different stress evolution path, but end up in the same final stress state as given in Fig. 5b. Another open question is, whether the 551 earthquake occurred (a) offshore on an undetected thrust Fault which connects the Roum Fault and the Akar Fault [59], (b) on the Roum Fault as assumed in our model [25, 27, 43], or (c) on the Jordan segment [15]. Future re-locations of historical earthquakes and a re-analysis of their magnitudes could change the results of both, the stress evolution, and thus the present-day stress state, and the assessment of the stress triggering hypothesis along the DSFS.

(2) *Data gaps in the historical earthquake catalogue:* This is relatively unlikely for the study area since it has been always densely populated [14,15]. A strong earthquake would have been described in historical documents and its impact would be reflected in historical buildings such as the impact of the earthquakes 1202, 1759a and 1837 on the crusader castle Vadum Jacob situated on the Jordan Fault [31] or archaeological excavations of the old city of Tiberias located at the Sea of Galilee [30]. However, it cannot be ruled out until a systematic investigation of the paleoseismicity in terms of trenches reveals more details on the historical seismic record along all fault segments.

(3) *The static stress transfer is not the major control for the sequence of earthquakes along the DSFS:* There is either an alternative stress transfer process which causes the earthquake sequence (e.g. visco-elastic relaxation) or there is no coherence between the earthquakes in our study area; that is, the earthquake sequence along the DSFS follows a Poisson distribution. This excites the question whether the DSFS is different in structure and/or in rheology in comparison to other continental transform faults where the hypothesis of static stress triggering has been tested successfully. Major differences are the neotectonics, the slip rates, and the earthquake recurrence rates. The latter two are approximately five times larger at the North Anatolian Fault [5, 60]. However, since our model for the ΔCFS analysis is time-independent, the lower slip rate cannot be responsible for our findings. A major structural difference compared to the North Anatolian Faults, the East Anatolian Faults, and the San Andreas Fault is the neotectonic regime of the DSFS. The tectonic regime changes from a releasing bend where the pull-apart basin of the Dead Sea Fault has been formed to the restraining bend of the Lebanon – Anti-Lebanon mountains. These two features are less than 200 km apart, have major influence on the kinematics, and probably control the unusual seismotectonics of the DSFS.

(4) *Transient stress transfer:* Transient stress changes due to visco-elastic relaxation processes are in the order of 0.1–1.0 MPa in the near field of the rupture plane on time scales varying in dependence of the viscosity of the lower crust and the upper mantle from a few years [61, 62] to hundreds of years [63]. Lorenzo-Martín et al. [64] applied for their stress evolution model of the North Anatolian Fault due to the 19th century strong earthquakes sequence a visco-elastic rheology with a linear viscosity of 5×10^{19} Pa s for the lower crust and 10^{18} Pa s for the lower crust. The resulting transient contribution to the stress changes e.g. on the Düzce segment was in average 0.2 MPa [64]. However, at the DSFS the contribution from transient processes to the total stress field evolution is probably small since the observed heat flow is in the order of 40 mW m^{-2} indicating a strong lower crust with high viscosities [65]. For large time scales (>100 years) stresses from tectonic loading and coseismic stress changes are probably predominant. For a fault slip rate of 5 mm/yr, the tectonic loading produces shear stress rates of ~0.003 MPa/yr. The coseismically induced static stress changes are in the order of ~5 MPa in the near-field earthquake rupture plane [5].

6. Conclusions

We tested the static stress triggering hypothesis using a sequence of 14 historical earthquakes along the central part of the DSFS and its stress evolution covering the time period from 551 to 2005. The stress triggering analysis revealed that about half of the earthquakes shows a possible triggering from the stress transfer of all previous earthquakes assuming a thresh-

old value of 0.01 MPa. The present-day stress state indicates that the Jordan segment has the highest potential to fail next. The accumulated ΔCFS stresses are >4 MPa on a ~90 km segment which could result in a M_S = 7.4 earthquake. Since six major cities (Beirut, Damascus, Haifa, Tel Aviv, Amman, and Jerusalem), are in close proximity at distances between 30 and 150 km from the Jordan segment, the seismic risk is probably underestimated. Given that the recurrence rates of devastating earthquakes as well as the magnitudes and locations of historical earthquakes are most important for the seismic hazard assessment in the DSFS, it is crucial to raise more data in order to undertake a more detailed analysis of stress evolution including a quantitative analysis of the uncertainties of the presented stress evolution model. To further constrain such models, and thus the seismic hazard potential, it is absolutely essential to increase the research on contemporary slip rates, e.g. from a dense continuous GPS network, estimation of geological slip rates for the Late Palaeocene and Holocene, and paleo-seismological research.

Acknowledgements

We especially thank Blanka Sperner, Karl Fuchs and John Reinecker for very constructive comments on an earlier version of this paper. We also thank the reviewer Shimon Wdowinski for constructive comments which improved the paper. The stress field calculation software Poly3D [49] and its graphical user interface Poly3DGUI from Frantz Maerten were provided by David Pollard from Stanford University. Figures were plotted with the Generic Mapping Tools [66]. We also acknowledge the support of the Deutsche Forschungsgemeinschaft (DFG, German Science Foundation) through the Collaborative Research Centre 461 (CRC 461) at the University of Karlsruhe, Germany: "Strong Earthquakes - a Challenge for Geosciences and Civil Engineering".

References

[1] R.A. Harris, Introduction to special section: stress triggers, stress shadows, and implications for seismic hazard, J. Geophys. Res. 103 (1998) 24347–24358.

[2] S. Steacy, J. Gomberg, M. Cocco, Introduction to special section: stress transfer, earthquake triggering, and time-dependent seismic hazard, J. Geophys. Res. 110 (2005), doi:10.1029/ 2005JB003692.

[3] S.S. Nalbant, J. McCloskey, S. Steacy, A.A. Barka, Stress accumulation and increased seismic risk in eastern Turkey, Earth Planet. Sci. Lett. 195 (2002) 291–298.

[4] S.S. Nalbant, A. Hubert, G.C.P. King, Stress coupling between earthquakes in northwest Turkey and the north Aegean Sea, J. Geophys. Res. 103 (1998) 24469–24486.

[5] R.S. Stein, A.A. Barka, J.H. Dietrich, Progressive failure on the North Anatolian fault since 1939 by earthquake stress triggering, Geophys. J. Int. 128 (1997) 594–604.

[6] F. Roth, Modelling of stress patterns along the western part of the Anatolian Fault Zone, Tectonophysics 152 (1988) 215–226.

[7] G. King, A. Hubert, S.S. Nalbant, B. Meyer, R. Armijo, D. Bowman, Coulomb interactions and the 17 August 1999 Izmit, Turkey earthquake, Earth Planet. Sci. Lett. 333 (2001) 557–569.

[8] J. Deng, L.R. Sykes, Evolution of the stress field in southern California and triggering of moderate-size earthquakes: a 200-year perspective, J. Geophys. Res. 102 (1997) 9859–9886.

[9] R.A. Harris, R.W. Simpson, In the shadow of 1857 – the effect of the great Ft. Tejon earthquake on subsequent earthquakes in southern California, Geophys. Res. Lett. 23 (1996) 229–232.

[10] R.A. Harris, R.W. Simpson, P.A. Reasenberg, Influence of static stress changes on earthquake locations in southern California, Nature 375 (1995) 221–224.

[11] T. Parsons, Recalculated probability of M ≥ 7 earthquakes beneath the Sea of Marmara, Turkey, J. Geophys. Res. 109 (2004), doi:10.1029/2003JB002667.

[12] J.R. Muller, A. Aydin, Using mechanical modeling to constrain fault geometries proposed for the northern Marmara Sea, J. Geophys. Res. 110 (2005), doi:10.1029/ 2004JB003226.

[13] S. Toda, R.S. Stein, K. Richards-Dinger, S.B. Bozkurt, Forecasting the evolution of seismicity in southern California: animations built on earthquake stress transfer, J. Geophys. Res. 110 (2005), doi:10.1029/ 2004JB003415.

[14] A. Ben-Menahem, Four thousand years of seismicity along the Dead Sea Rift, J. Geophys. Res. 96 (1991) 20195–20216.

[15] N.N. Ambraseys, C.P. Melville, R.D. Adams, The Seismicity of Egypt, Arabia and the Red Sea, University Press, Cambridge, 1994.

[16] S. Marco, A. Agnon, High-resolution stratigraphy reveals repeated earthquake faulting in the Masada Fault Zone, Dead Sea Transform, Tectonophysics 408 (2005) 101–112.

[17] Z.B. Begin, D.M. Steinberg, G.A. Ichinose, S. Marco, A 40,000 year unchanging seismic regime in the Dead Sea Rift, Geol. Soc. Am. 334 (2005), doi:10.1130/ G21115.1.

[18] C. Migowski, A. Agnon, R. Bookman, J.F.W. Negendank, M. Stein, Recurrence pattern of Holocene earthquakes along the Dead Sea Transform revealed by varve-counting and radiocarbon dating of lacustrine sediments, Earth Planet. Sci. Lett. 222 (2004) 301–314.

[19] S. Marco, T.K. Rockwell, A. Agnon, A. Heimann, U. Frieslander, Late Holocene slip of the Dead Sea Transform revealed in 3D paleoseismic trenches on the Jordan Gorge Fault, Earth Planet. Sci. Lett. 234 (2005) 189–2005.

[20] S. Wdowinski, Y. Bock, G. Baer, L. Prawirodirdjo, N. Bechor, S. Naaman, R. Knafo, Y. Forrai, Y. Melzer, GPS measurements of current crustal movement along the Dead Sea Fault, J. Geophys. Res. 109 (2004), doi:10.1029/2003JB002640.

[21] Z. Garfunkel, Internal structure of the Dead Sea leaky transform (rift) in relation to plate kinematics, Tectonophysics 80 (1981) 81–108.

[22] R.W.H. Butler, S. Spencer, H.M. Griffiths, The structural response to evolving plate kinematics during transpression: evolution of the Lebanese restraining bend of the Dead Sea Transform, in: R.E. Holdsworth, R.A. Strachan, J.F. Dewey (Eds.), Continental Transpressional and Transtensional Tectonics, Special Publication, vol. 135, Geological Society, London, 1998, pp. 81–106.

[23] Y. Klinger, J.P. Avouac, N. Abou Karaki, L. Dorbath, D. Bourles, Slip rate on the Dead Sea Transform fault in northern Araba Valley (Jordan), Geophys. J. Int. 142 (2000) 755–768.

[24] N.N. Ambraseys, The earthquake of 1 January 1837 in Southern Lebanon and Northern Israel, Ann. Geofis. 40 (1997) 923–936.

[25] R. Darawcheh, M.R. Sbeinati, C. Margottini, S. Paolini, The 9 July 551 AD Beirut earthquake, Eastern Mediterranean region, J. Earthqu. Eng. 4 (2000) 403–414.

[26] D.H.K. Amiran, E. Arieh, D.L. Turcotte, Earthquakes in Israel and adjacent areas: macroseismic observations since 100 B.C.E., Israel, Explor. 44 (1994) 260–305.

[27] K. Khair, G.F. Karakaisis, E.E. Papadimitriou, Seismic zonation of the Dead Sea Transform fault area, Ann. Geofis. 43 (2000) 61–79.

[28] N.N. Ambraseys, C.P. Melville, An analysis of the eastern Mediterranean earthquake of 20 May 1202, in: H. Meyer, K. Shimazaki, B. Lee (Eds.), Historical Seismograms and Earthquakes of the World, Academic Press, San Diego, California, 1988, pp. 181–200.

[29] N.N. Ambraseys, M. Barazangi, The 1759 earthquake in the Bekaa Valley: implications for earthquake hazard assessment in the Eastern Mediterranean Region, J. Geophys. Res. 94 (1989) 4007–4013.

[30] S. Marco, M. Hartal, N. Hazan, L. Lev, M. Stein, Archaeology, history, and geology of the A.D. 749 earthquake, Dead Sea Transform, Geology 8 (2003) 665–668.

[31] R. Ellenblum, S. Marco, A. Agnon, T.K. Rockwell, A. Boas, Crusader castle torn apart by earthquake at dawn, 20 May 1202, Geology 26 (1998) 303–306.

[32] M. Meghraoui, F. Gomez, R. Sbeinati, J. van der Woerd, M. Mouty, A.N. Darkal, Y. Radwan, I. Layyous, H. Al Najjar, R. Darawcheh, F. Hijazi, R. Al-Ghazzi, M. Barazangi, Evidence for 830 years of seismic quiescence from paleoseismology, archae-oseismology and historical seismicity along the Dead Sea Fault in Syria, Tectonophysics 210 (2003) 35–52.

[33] Z. Garfunkel, I. Zak, R. Freund, Active faulting in the Dead Sea Rift, Tectonophysics 80 (1981) 1–26.

[34] Z. Ben-Avraham, Structural framework of the Gulf of Elat (Aqaba) – northern Red Sea, J. Geophys. Res. 90 (1985).

[35] R. Freund, I. Zak, Z. Garfunkel, Age and rate of the of the sinistral movement along the Dead Sea Rift, Nature 220 (1968) 253–255.

[36] A.M. uennell, The structural and geomorphic evolution of the Dead Sea Rift, . J. Geol. Soc. Lond. 114 (1958) 1–24.

[37] R. Westaway, Present-day kinematics of the Middle East and eastern Mediterranean, J. Geophys. Res. 99 (1994) 12071–12090.

[38] M. Daëron, L. Benedetti, P. Tapponnier, A. Sursock, R.C. Finkel, Constraints on the post ~25-ka slip rate of the Yammouneh Fault (Lebanon) using in situ cosmogenic ^{36}Cl dating of offset limestone–clast fans, Earth Planet. Sci. Lett. 227 (2004) 105–119.

[39] R.W.H. Butler, S. Spencer, H.M. Griffiths, Transcurrent fault activity on the Dead Sea Transform in Lebanon and its implication for plate tectonics and seismic hazard, J. Geol. Soc. 154 (1997) 757–760.

[40] F. Gomez, M. Meghraoui, A.N. Darkal, R. Sbeinati, R. Darawcheh, C. Tabet, M. Khawlie, M. Charabe, K. Khair, M. Barazangi, Coseismic displacements along the Serghaya Fault: an active branch of the Dead Sea Fault System in Syria and Lebanon, J. Geol. Soc. 158 (2001) 405–408.

[41] C.D. Walley, A braided strike–slip model for the northern continuation of the Dead Sea Fault and its implications for Levantine tectonics, Tectonophysics 145 (1988) 63–72.

[42] H.M. Griffiths, R.A. Clark, K.M. Thorp, S. Spencer, Strain accommodation at the lateral margin of an active transpressive zone: geological and seismological evidence from the Lebanese restraining bend, J. Geol. Soc. 157 (2000) 289–302.

[43] K. Khair, Geomorphology and seismicity of the Roum Fault as one of the active branches of Dead Sea Fault System in Lebanon, J. Geophys. Res. 106 (2001) 4233–4245.

[44] Y. Ben-Gai, Z. Ben-Avraham, Tectonic processes in offshore northern Israel and the evolution of the Carmel Structure, Mar. Pet. Geol. 12 (1995) 533–548.

[45] Z. Ben-Avraham, J.K. Hall, Geophysical survey of Mount Carmel structure and its extension into the eastern Mediterranean, J. Geophys. Res. 82 (1977) 793–802.

[46] N.N. Ambraseys, J.A. Jackson, Faulting associated with historical and recent earthquakes in the Eastern Mediterranean region, Geophys. J. Int. 133 (1998) 390–406.

[47] T. van Eck, A. Hofstetter, Fault geometry and spatial clustering of microearthquakes along the Dead Sea–Jordan Rift fault zone, Tectonophysics 180 (1990) 15–27.

[48] A. Shapira, A. Hofstetter, Source parameters and scaling relationships of earthquakes in Israel, Tectonophysics 217 (1993) 217–226.

[49] A.L. Thomas, Poly3D: a three-dimensional, polygonal element, displacement discontinuity boundary element computer program with applications to fractures, faults, and cavities in the earth's crust, MS thesis, Stanford California, 1993.

[50] Z. Ben-Avraham, U. ten Brink, R. Bell, M. Reznikov, Gravity field over the Sea of Galilee: evidence for a composite basin along a transform fault, J. Geophys. Res. 101 (1996) 533–544.

[51] P.A. Reasenberg, R.W. Simpson, Response of regional seismicity to the static stress change produced by the Loma Prieta earthquake, Science 255 (1992) 1687–1690.
[52] E. Zilberman, R. Amit, N. Porat, Y. Enzel, U. Avner, Surface rupture induced by the devastating 1068 AD earthquake in the Arava Valley, Dead Sea Rift, Israel, Tectonophysics 408 (2005) 79–99.
[53] Y. Klinger, J.P. Avouac, L. Dorbath, N. Abou Karaki, N. Tisnerat, Seismic behaviour of the Dead Sea Fault along Araba Valley, Jordan, Geophys. J. Int. 142 (2000) 769–782.
[54] E. Guidoboni, F. Bernardini, A. Cosmastri, The 1138–1139 and 1156–1159 destructive seismic crises in Syria, south-eastern Turkey and northern Lebanon, J. Seismol. 8 (2004) 105–127.
[55] R.A. Harris, R.W. Simpson, Suppression of large earthquakes by stress shadows: a comparison of Coulomb and rate-and-state failure, J. Geophys. Res. 103 (1998) 24439–24451.
[56] H. Horikawa, Earthquake doublet in Kagoshima, Japan: rupture of asperities in a stress shadow, Bull. Seismol. Soc. Am. 91 (2001) 112–127.
[57] Y.G. Wan, Z.L. Wu, G.W. Zhou, Focal mechanism dependence of static stress triggering of earthquakes, Tectonophysics 390 (2004) 235–243.
[58] M. Daëron, Y. Klinger, P. Tapponnier, A. Elias, E. Jacques, A. Sursock, Sources of the large A.D. 1202 and 1759 Near East earthquakes, Geology 33 (2005), doi:10.1130/G21352.1.
[59] A. Elias, P. Tapponnier, G. King, S.K. Singh, A. Sursock, A. Briais, H. Carton, E. Jacques, M. Daëron, R. Jomaa, Fresh submarine seismic breaks due to historical thrust earthquakes offshore Lebanon, Eos, Trans. - Am. Geophys. Union 85 (47) (2004) Abstract T13C–1382.
[60] S. McClusky, S. Balassanian, A. Barka, C. Demir, S. Ergintav, Georgiev, O. Gurkan, M. Hamburger, K. Hurst, H. Kahle, K. Kastens, G. Kekelidze, R. King, V. Kotzev, O. Lenk, S. Mahmoud, Mishin, M. Nadariya, A. Ouzounis, D. Paradissis, Y. Peter, M. Prilepin, R. Reilinger, I. Sanli, H. Seeger, A. Tealab, M.N. Toks z, G. Veis, Global positioning system constraints on plate kinematics and dynamics in the eastern Mediterranean and Caucasus, J. Geophys. Res. 105 (2000) 5695–5719.
[61] A.M. Freed, J. Lin, Delayed triggering of the 1999 Hector Mine earthquake by viscoelastic stress transfer, Nature 411 (2001) 180–183.
[62] T. Hergert, O. Heidbach, New insights in the mechanism of postseismic stress relaxation exemplified by the June 23rd 2001 M_w =8.4 earthquake in southern Peru, Geophys. Res. Lett. 33 (2006), doi:10.1029/2005GL024585.
[63] Li, M. Liu, E. Sandvol, Stress evolution following the 1811–1812 large earthquakes in the New Madrid Seismic Zone, Geophys. Res. Lett. 32 (2005), doi:10.1029/2004GL022133.
[64] F. Lorenzo-Martin, F. Roth, R. Wang, Elastic and inelastic triggering of earthquakes in the North Anatolian Fault zone, Tectonophysics 424 (2006) 271–289.
[65] F. Alderson, Z. Ben-Avraham, A. Hofstetter, E. Kissling, T. Al-Yazjeen, Lower-crustal strength under the Dead Sea basin from local earthquake data and rheological modeling, Earth Planet. Sci. Lett. 214 (2003) 129–142.
[66] P. Wessel, W.H.F. Smith, New, improved version of Generic Mapping Tools released, Eos, Trans. - Am. Geophys. Union 79 (1998) 579.